

Unusually high-density 2D electron gases in N-polar AlGa_N/Ga_N heterostructures with Ga_N/AlN superlattice back barriers grown on sapphire substrates

Maciej Matys,^{a)} Atsushi Yamada, and Toshihiro Ohki
Fujitsu Limited, Kawasaki, Kanagawa, 211-8588, Japan

(Dated: 28 November 2024)

We reported on the observation of extremely high-density ($> 10^{14}\text{cm}^{-2}$) 2D electron gas in N-polar AlGa_N/Ga_N heterostructures grown on sapphire substrates. Due to introducing the Ga_N/AlN superlattice (SL) back barrier between the Ga_N buffer layer and AlGa_N barrier layer, we observed a giant enhancement of the 2D electron gas density at the Ga_N/AlGa_N interface from $3 \times 10^{13}\text{cm}^{-2}$ (without SL) to $1.4 \times 10^{14}\text{cm}^{-2}$ (with SL back barrier) that is only one order of magnitude below the intrinsic crystal limit of $\approx 10^{15}\text{cm}^{-2}$. We found that the changes of 2D electron gas density with SL correlated well with the changes of the wafer warp parameter which suggests that the strains are responsible for the 2D electron gas density enhancement (reduction of the piezoelectric polarization in the Ga_N channel). Nevertheless, this finding is probably insufficient to fully explain the observed high 2D electron gas density. Simultaneously, the room temperature electron mobility was $169\text{ cm}^2/\text{Vs}$, which with the electron density of $1.4 \times 10^{14}\text{cm}^{-2}$ gives a low sheet resistance of $264\ \Omega/\text{sq}$ (one of the lowest reported so far for the N-polar 2D electron gas channel). Finally, the possibility of application of such high-density 2D electron gas with low sheet resistance to transistors, emitters and detectors was discussed.

The discovery of the high-conductivity quantum-confined two-dimensional (2D) electron gases at the interface of AlGa_N/Ga_N semiconductor heterostructures in the mid-1990s¹⁶ has generated considerable attention in the scientific community since its formation did not require the presence of chemical dopants. Contrary to AlGaAs/GaAs material systems²⁻⁴, 2D electron gases in AlGa_N/Ga_N heterostructures are formed spontaneously due to net polarization charges composed of spontaneous and piezoelectric polarization of AlGa_N and Ga_N^{5,6}.

Recently, the N-polar III-nitride heterostructures attracted great attention in nitride community due to their several advantages over metal-polar counterpart in high frequency and high-power applications⁷⁻¹³. The typical as-grown 2D electron gas density in N-polar III-nitride heterostructures ranging from low- 5×10^{12} to high $3 \times 10^{13}\text{cm}^{-2}$ with mobility between $300\text{--}2500\text{ cm}^2/\text{Vs}$ and sheet resistances from 150 to $600\ \Omega/\text{sq}$ ^{7,14-18}. However, it should be highlighted the highest observed 2D electron gas densities in N-polar III-nitride heterostructures were $4.3 \times 10^{13}\text{cm}^{-2}$ with mobility $450\text{ cm}^2/\text{Vs}$ and sheet resistance $320\ \Omega/\text{sq}$ ^{14,15}. Such gases were realized using a high Al-content AlGa_N barrier and AlN substrates^{14,15}. The 2D electron densities higher than 10^{14}cm^{-2} have not been measured in N-polar III-nitride semiconductor heterostructures so far in an as-grown structure or field-effect induced channel.

In this work, the extremely high-2D electron densities ($> 10^{14}\text{cm}^{-2}$) are demonstrated in N-polar AlGa_N/Ga_N heterostructure. It was found that introducing the Ga_N/AlN superlattice (SL) back barrier be-

tween Ga_N buffer layer and AlGa_N barrier layer leads to a giant enhancement of 2D electron gas density at Ga_N/AlGa_N interface. In particular, we observed an increase of 2D electron gas density from $3 \times 10^{13}\text{cm}^{-2}$ (without SL structure) to $1.4 \times 10^{14}\text{cm}^{-2}$ (with SL) that is only an order of magnitude below the intrinsic crystal limit of $\approx 10^{15}\text{cm}^{-2}$. The Hall measurement shows that this high-2D electron gas density has a room temperature electron mobility as $169\text{ cm}^2/\text{Vs}$ which with 2D electron gas density of $1.4 \times 10^{14}\text{cm}^{-2}$ leads to a very low sheet resistance of $264\ \Omega/\text{sq}$.

Fig. 1(a) shows the schematic illustration of the fabricated N-polar AlGa_N/Ga_N heterostructures. The investigated structures were grown by Metal-Organic Chemical Vapour Deposition (MOCVD) using trimethylgallium (TMGa), trimethylaluminum (TMAI), and ammonia as precursors on (0001) sapphire with a misorientation angle of 4° toward the a-sapphire-plane. Firstly, a 100 nm AlN layer was grown at $1025\text{ }^\circ\text{C}$ with a rate of $2\ \mu\text{m}/\text{h}$. Subsequently, a 400 nm unintentionally doped Ga_N buffer layer was grown at $1025\text{ }^\circ\text{C}$ with a V/III ratio of 1600 at the pressure of 20 kPa. On top of the buffer Ga_N layer a thin superlattice (SL) structure was deposited, which contains the alternating Ga_N and AlN layers (see inset of Fig. 1(a)). The thickness of Ga_N and AlN layers in SL structure was 10 and 5 nm, respectively. The number of SL periods, n , (inset of Fig. 1(a)) was varying between 0 to 10. Next, a 30-nm-thick Al_{0.3}Ga_{0.7}N barrier layer was deposited followed by a 20 nm thick undoped Ga_N channel layer. Finally, 3-nm-thick Al_{0.4}Ga_{0.6}N and 2-nm-thick Ga_N cap layers were grown on the top of the structure. The polarity of the fabricated N-polar AlGa_N/Ga_N heterostructures was confirmed by the KOH etching and X-ray diffraction (XRD) measurements (not shown). The transmission electron microscope (TEM)

^{a)}Fujitsu Limited, Kawasaki, Kanagawa, 211-8588, Japan; Electronic mail: matys.maciej@fujitsu.com

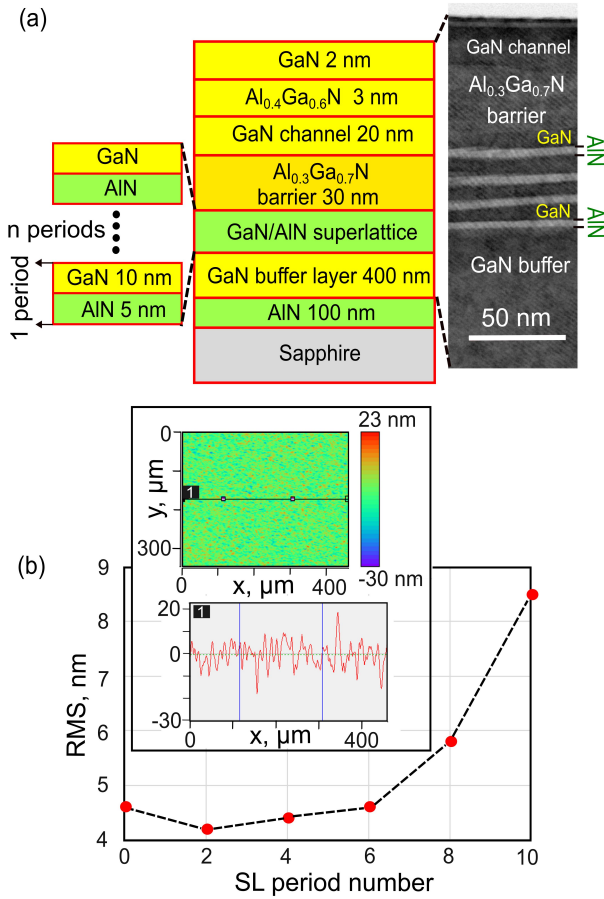


FIG. 1. (a) Schematic illustration of the fabricated epitaxial structures used in this study. (b) Root mean square (RMS) roughness as a function of SL periods. Inset of (a) shows the TEM image of the AlGaN/GaN heterostructure with 4 period GaN/AlN SL structure. Inset of (b) shows the 2D and 1D surface profiles from interferometric surface profilers of the AlGaN/GaN heterostructure with 4 period GaN/AlN SL

image confirmed that the AlN/GaN SL structure was successfully grown (see inset of Fig. 1(a)). The surface morphologies of the fabricated N-polar AlGaN/GaN heterostructures were measured using interferometric surface profiler. The measurement from the large area over $400 \mu\text{m} \times 300 \mu\text{m}$ indicates the smooth morphology with a root mean square (*RMS*) roughness between 4.2 to 4.5 nm for 0 to 6 period SL as shown in Fig. 1(b). However above 6 period SL, the surface becomes very rough with *RMS* value of 8.5 nm for 10 period SL (Fig. 1(b)).

To characterize the electron transport properties in the fabricated N-polar AlGaN/GaN heterostructures, we applied the Hall-effect measurements with the Van der Pauw method using the aluminum-titanium Ohmic contacts and the magnetic field of 1 T. Fig. 2(a) and (b) show the measured room temperature 2D electron density and mobility as a function of the SL period number. Without SL structure the N-polar AlGaN/GaN heterostructures exhibits the 2D electron gas density of

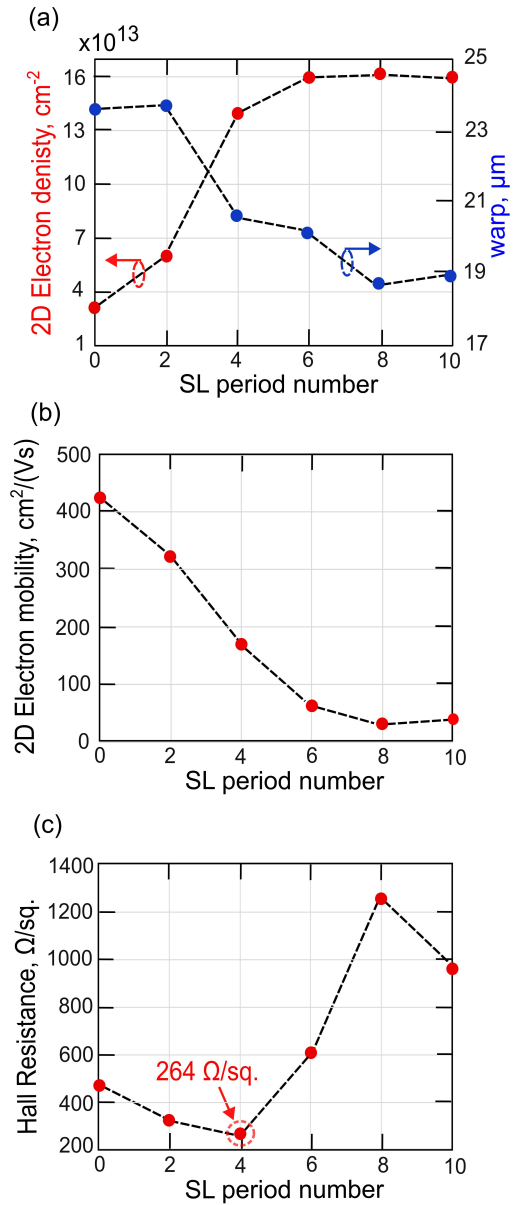


FIG. 2. (a) Room-temperature 2D electron gas density as a function of the SL period number, (b) room-temperature electron mobility vs. SL period number and (c) room-temperature Hall sheet resistance as a function of the SL period number. Inset of (a) shows schematically illustration of the warp parameter.

$3 \times 10^{13} \text{cm}^{-2}$ with mobility of $440 \text{cm}^2/\text{Vs}$. The mobility value of $440 \text{cm}^2/\text{Vs}$ is relatively low due to the non-uniformity of AlN/GaN SL (see the TEM image, inset of Fig. 1(a)) which arises as a result of the growth on the sapphire substrate with a miscut angle orientation. By increasing the SL period number, the 2D electron gas density initially slowly increases and then jumps rapidly at 4 period SL reaching the concentration of $1.4 \times 10^{13} \text{cm}^{-2}$ (see Fig. 2(a)). Further, the increasing of SL periods leads to the saturation of the electron gas

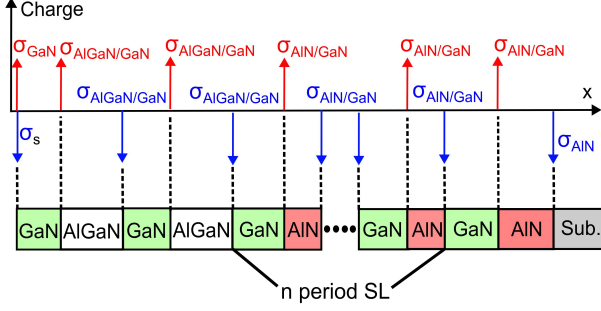


FIG. 3. Distribution of polarization charges in the investigated SL based N-polar AlGaIn/GaN heterostructures.

density at the level $1.4 \times 10^{13} \text{cm}^{-2}$. Simultaneously, the electron mobility decreases with increasing of SL periods up to 8 and then becomes constant (Fig. 2(b)). We attributed this effect to the interface roughness scattering mechanism. In particular, Singiseti et al.¹⁷ showed that the interface roughness is a dominant scattering mechanism limiting the electron mobility in the N-polar GaN quantum well channels. On the other hand, the interface roughness scattering is proportional to the square of the electric field which is likely to increase in the region of GaN/AlGaIn interface with increasing the SL period number. Fig. 2(c) shows the room temperature Hall sheet resistance (R_H) as a function of the SL period number. As can be seen, R_H exhibits a U-shaped dependency on the SL period number, namely with increasing n , R_H gradually decreases reaching the minimum at 4 period SL and subsequently increases. In the range from 0 to 4 period SL, R_H decreases almost 2 times which is a direct consequence of the rapid increasing of the 2D electron gas density (Fig. 2(a)). On the other hand, in the range from 4 to 8 period SL, R_H increases approximately 4.5 times. This increases is due to the fact that the 2D electron density is practically saturated in the range from 4 to 8 period SL. However, the electron mobility in this range still continues decreasing from 169 at 4 period SL to $80 \text{cm}^2/\text{Vs}$ at 8 period SL (Fig. 2(b)).

To explain the above results, we performed the Technology Computer Aided Design (TCAD) simulations of the band diagram of investigated heterostructures. In the simulation, we assumed the polarization charges (σ) at AlN/GaN, $\text{Al}_{0.3}\text{Ga}_{0.7}\text{N}/\text{GaN}$ and $\text{Al}_{0.4}\text{Ga}_{0.6}\text{N}/\text{GaN}$ interfaces given by the following equation⁵:

$$\frac{\sigma}{q} = 6.41 \times 10^{13} - 1.17 \times 10^{13}x(1-x) \quad (1)$$

where σ is in the unit of cm^{-2} and x is the Al composition. In addition, we assumed that on the GaN surface the positive spontaneous polarization charge of $\sigma_{\text{GaN}} = 1.8 \times 10^{13} \text{cm}^{-2}$ is compensated by the surface negative charge $\sigma_s = -1.8 \times 10^{13} \text{cm}^{-2}$. Such compensation charge was previously found on the N-polar GaN surface by the X-ray photoelectron spectroscopy

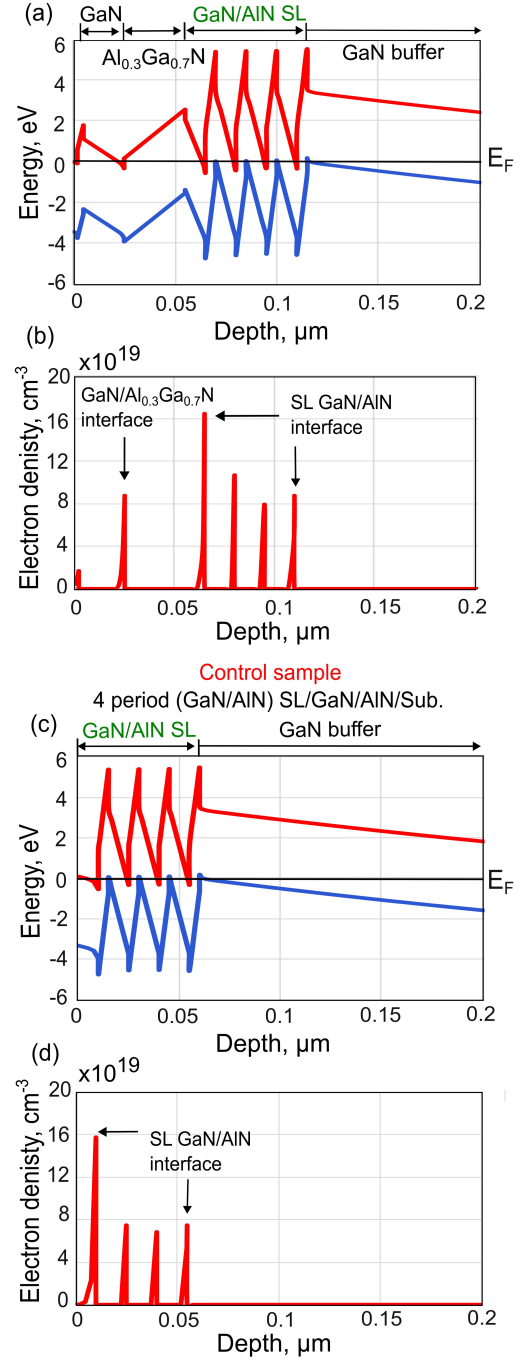


FIG. 4. Simulated (a) band diagram and (b) electron density of AlGaIn/GaN heterostructure with 4 period GaN/AlN SL structure. Simulated (c) band diagram and (d) electron density of the control sample, i.e., 4-period (GaN/AlN) SL/GaN (400 nm)/AlN (100 nm)/sapphire.

measurements¹⁹. The detailed distribution of the assumed polarization charges in the heterostructure is shown in Fig. 3.

The band diagram simulation clearly shows that in addition to the 2D electron channel at the GaN/AlGaIn interface, the high-density 2D electron gases should be

formed in the SL structure (see Figs. 4(a) and (b)). The formation of the parallel 2D electron channels in the SL structure could explain a significant increase of the 2D electron gas density between 0 and 4 period SL (Fig. 2(a)). However, the saturation of 2D electron gas density between 4 to 10 period SL is the signature that 2D electron gas is not formed in the SL structure (2D electron gas density should depend on the SL periods number approximately linearly, as it was reported previously). To confirm no 2D electron gases in the SL structure we grew the control sample i.e. 4-period SL/GaN (400 nm)/AlN (100 nm)/Sapphire. The band diagram simulations indicated that the SL structure in the control sample should contain the similar very high density-2D electron gas as investigated ones (see Figs. 4(c) and (d)). However, the Hall-effect measurements from the control sample shows high contactless sheet resistance of 710 Ohm/s, which is similar to the sheet resistance of the 400 nm N-polar GaN layer (800 Ohm/sq). This means that 2D electron gas was not formed in the SL structure. One of the reasons why the 2D electron gas in the SL structure is not observed may be the fact that AlN in the SL is not pure AlN but a high content AlGaN. For example, if instead of the AlN layer the $\text{Al}_{0.6}\text{Ga}_{0.4}\text{N}$ layer has been formed in SL the 2D electron gas should not appear, as shown in Figs. 5(a) and (b). Another reason of the high-resistivity of SL structure can be existence of acceptor traps at negative polarization interfaces of SL⁷. In light of the lack of a 2D electron gases in SL structure we can assume that the carrier transport in the investigated heterostructures (Fig. 1(a)) was mainly by the 2D electron gas at the GaN/ $\text{Al}_{0.3}\text{Ga}_{0.7}\text{N}$ interface. However it should be noted that besides 2D electron channel at the GaN/ $\text{Al}_{0.3}\text{Ga}_{0.7}\text{N}$ interface there is also some 2D electron channel in GaN cap layer (see Figs 5(a) and (b)). According to the TCAD simulation this 2D electron gas has totally negligible concentration compare to the 2D electron gas at the GaN/ $\text{Al}_{0.3}\text{Ga}_{0.7}\text{N}$ interface (Fig. 5(b)). Thus it can be concluded that carrier transport was entirely dominant by the 2D electron gas at the GaN/ $\text{Al}_{0.3}\text{Ga}_{0.7}\text{N}$ interface.

After excluding the formation of 2D electron gas in the SL structure another reason for enhancement of 2D electron gas density needs to be identified. The enhancement of the stress due to SL deposition is a natural factor that could cause increasing of the 2D electron gas. For example, previously K.-S. Im et al.²⁰ reported a giant formation of 2D electron gas density $> 10^{14}\text{cm}^{-2}$ in the metal-polar AlGaIn/GaN heterostructure on Si substrates by generation of a strong tensile stress. To estimate roughly the strain in our heterostructures we measured the standardized warp parameter (flatness of the wafer) as shown in Fig. 2(a). One can note that the dependencies of the warp parameter as a function of the SL period number is strikingly similar to the dependence of 2D electron gas vs. SL period number. In particular, the biggest changes of the warp parameter occur between 2 and 4 period SL, where the giant enhancement of 2D

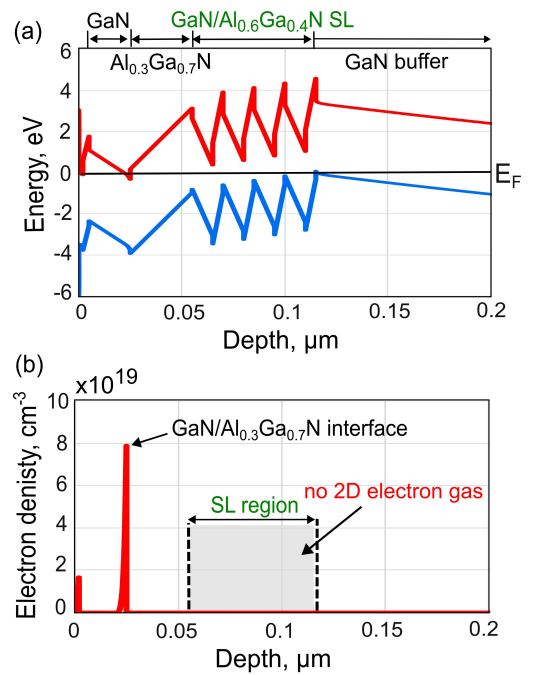


FIG. 5. Simulated (a) band diagram and (b) electron density of AlGaIn/GaN heterostructure with 4 period GaN/ $\text{Al}_{0.6}\text{Ga}_{0.4}\text{N}$ SL structure.

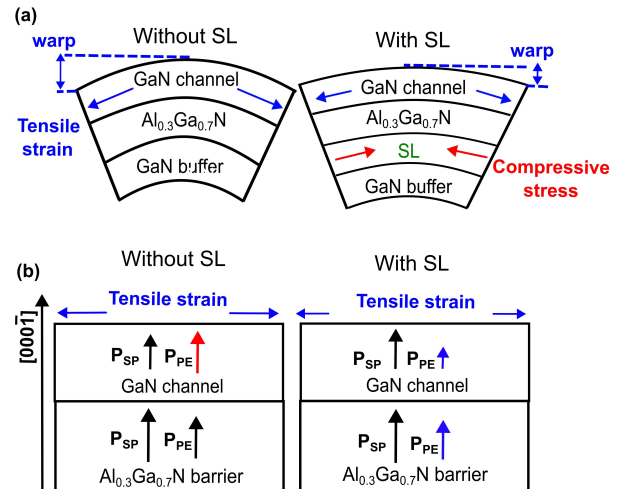


FIG. 6. (a) Schematic illustration of warp parameter reduction in the investigated epitaxial structures. (b) Directions of the spontaneous and piezoelectric polarizations in the examined structures. Enhancement of 2D electron density at the GaN/ $\text{Al}_{0.3}\text{Ga}_{0.7}\text{N}$ interface occurred due to reduction of P_{PE} in GaN channel after SL deposition.

electron gas density takes place (Fig. 2(a)). Decreasing of the warp parameter in the range between 2 and 4 period SL indicates that the wafer becomes more flatter. On the other hand the bow parameter was positive which means that the curvature of the wafer was concave. Thus the wafer flattening occurred probably due to the gener-

ation of compressive stress in SL structure which reduced tensile strain as schematically shown in Fig. 6(a). The reduction of tensile strains can lead to enhancement of the 2D electron density at the GaN/Al_{0.3}Ga_{0.7}N interface in the following manner. Firstly we recall the definition of the piezoelectric polarization P_{PE} vector

$$P_{PE} = 2\epsilon_{xx}\left(\frac{e_{31} - e_{33}C_{13}}{C_{33}}\right) \quad (2)$$

where e_{31} and e_{33} are the piezoelectric coefficients, ϵ_{xx} is the in-plane component of the strain tensor, and C_{13} and C_{33} are components of the compliance tensor.

From above equation it follows that if the GaN layer is under the tensile strain, P_{PE} vector in GaN channel has the same direction as spontaneous polarization ones P_{SP} (see Fig. 6(b)) since the factor $\epsilon_{xx}\left(\frac{e_{31}-e_{33}C_{13}}{C_{33}}\right) > 0$. This means that P_{PE} according to Fig. 6(b) decreases 2D electron gas density at the GaN/Al_{0.3}Ga_{0.7}N interface. On the other hand as we mentioned before the tensile strain become reduced when SL is deposited (Fig. 6(a)). Thus in the AlGaN/GaN heterostructures with SL, P_{PE} in GaN channel should be lower than in the structures without SL (see Fig. 6(b)). If we assumed now that decreases of P_{PE} in Al_{0.3}Ga_{0.7}N barrier layer after deposited of SL is much lower in the case of GaN channel (Fig. 6 (b)) then enhancement of 2D electron density at the GaN/Al_{0.3}Ga_{0.7}N interface will occur due to reduction of P_{PE} in GaN channel. However there is one weak point of this explanation: changes of P_{PE} in GaN channel itself may be too weak to induced such huge 2D electron density (Fig. 2(a)). Thus we believe that there are other stress-related contributions leading to enhancement of the 2D electron density at GaN/Al_{0.3}Ga_{0.7}N interface. Another factor which could enhance the 2D electron density is that introduced SL may act as excellent electron blocking layers suppressing the escape of electrons from quantum well at GaN/Al_{0.3}Ga_{0.7}N interface.

Fig. 7 shows the benchmark plot comparing the 2D electron gas densities obtained in this work with the as-grown single-2D electron gases reported in the literature for N-polar III-nitride semiconductor heterostructures on various substrates: SiC, Sapphire, GaN and AlN. The GaN/AlGaN 2D electron gases fabricated in this work exhibit the highest densities among all N-polar III-nitride heterostructures: they are more than three times larger than highest 2D electron gases observed so far in N-polar III-nitride heterostructures grown on AlN substrates and only an order of magnitude below the intrinsic crystal limit of $\approx 10^{15}\text{cm}^{-2}$. Furthermore, in the case of 4 period SL, R_H reach 269 Ohm/sq which is one of the lowest reported to date for N-polar 2D electron gas channel.

In the context of the device applications, the high-density 2D electron gas can be highly desired²¹. In particular, the high-density 2DEG reduces the parasitic series resistances in the source/drain region which leads to an increasing of the on-currents, transconductance and, in consequence, the power output. For example,

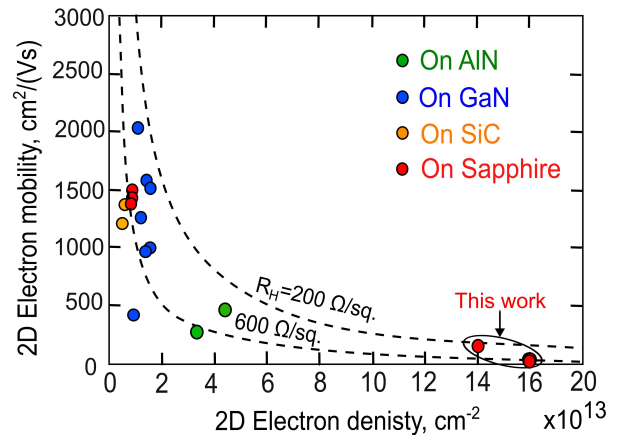


FIG. 7. Room-temperature electron density and mobility reported in N polar III-nitride semiconductor heterostructures grown on various substrates: sapphire, GaN and AlN^{7,14-18}.

K.-S. Im et al.²⁰ used the extremely high-density 2DEG ($> 10^{14}\text{cm}^{-2}$) as a source and drain in the Ga-polar GaN metal-oxide-semiconductor field-effect transistor (MOSFET) (which was based on the AlGaN/GaN heterostructure). Due to this, the authors were able to realize a high drain current and extrinsic transconductance. In addition, a high-density 2DEG may reduce the effect of the surface and buffer traps^{22,23}. Beside the transistor applications, high-density 2DEG systems are also attractive for infrared plasmonic applications^{24,25} or “charge gain” devices^{26,27}. In particular, there are many reports about the application of AlGaN/GaN heterostructures in terahertz plasmonic sources and detectors²⁸⁻³⁴. It is obvious that the extremely high-density 2DEG can significantly boost the performance of these devices (since the frequency of 2D plasmons is proportional to 2D electron concentration). Thus, the ability of realization of N-polar III-nitride heterostructures with very high-density 2DEG may be desirable for various device applications.

In summary, we reported on the observation of the extremely high-density 2D electron gas in N-polar AlGaN/GaN heterostructures grown on sapphire substrates. We found that the introduction of the GaN/AlN superlattice back barrier between the GaN buffer layer and AlGaN barrier layer leads to a giant enhancement of 2DEG density at the GaN/AlGaN interface from $3 \times 10^{13}\text{cm}^{-2}$ (without SL) to $1.4 \times 10^{14}\text{cm}^{-2}$. The increase of 2DEG density correlated well with the changes of the wafer warp parameter, which suggested that the strains are responsible for the enhancement of 2DEG density. More precisely, SL increases compressive stress which leads to a reduction of tensile strain and piezoelectric polarization in the GaN channel layer. However, the changes in piezoelectric polarization of GaN channel layer solely are probably insufficient to fully explain the observed extremely high density of 2DEG. Simultaneously, the room temperature electron mobility (at the 2D electron gas densities $1.4 \times 10^{14}\text{cm}^{-2}$) was $169\text{cm}^2/\text{Vs}$

which led to the low Hall sheet resistance of 264 Ohm/sq (one of the lowest reported so far for N-polar 2D electron gas channel).

ACKNOWLEDGMENTS

The authors express gratitude to Norikazu Nakamura for his kind support and discussions. The authors would like to thank Yoshiharu Kinoue and Takaaki Sakuyama for their support in experiments.

- ¹M.A. Khan, J.N. Kuznia, J.M. Van Hove, N. Pan, J. Carter, *Appl. Phys. Lett.* **60**(24), 3027–3029 (1992)
- ²H. Hasegawa, M. Akazawa *Applied Surface Science* **254** 8005–8015 (2008).
- ³H. Hasegawa, M. Akazawa, A. Domanowska, B. Adamowicz, *Applied Surface Science* **256** 5698–5707 (2010).
- ⁴H. Hasegawa, M. Akazawa, *Applied Surface Science* **255** 628–63 (2008).
- ⁵O. Ambacher, J. Smart, J. R. Shealy, N. G. Weimann, K. Chu, M. Murphy, W. J. Schaff, L. F. Eastman, R. Dimitrov, L. Wittmer, M. Stutzmann, W. Rieger, J. Hilsenbeck, *J. Appl. Phys.* **85**, 3222, (1999).
- ⁶F. Bernardini, V. Fiorentini, D. Vanderbilt, *Phys. Rev. B: Condens. Matter Mater. Phys.* **56**, R10024–R10027 (1997).
- ⁷S. Rajan; A. Chini; M. Wong; J. Speck; U. Mishra *J. Appl. Phys.* **102**, 044501 (2007).
- ⁸B. Romanczyk, S. Wienecke, M. Guidry, H. Li, K. Hestroffer, E. Ahmadi, X. Zheng, S. Keller, U.K. Mishra 2016 74th Annual Device Research Conference (DRC) (IEEE), pp. 1-2 (2016).
- ⁹B. Romanczyk, U.K. Mishra, X. Zheng, M. Guidry, H. Li, N. Hatui, C. Wurm, A. Krishna, E. Ahmadi, S. Keller *IEEE Electron. Device Lett.*, **41**, pp. 349-352 (2020).
- ¹⁰B. Romanczyk, S. Wienecke, M. Guidry, H. Li, E. Ahmadi, X. Zheng, S. Keller, U.K. Mishra *IEEE Trans. Electron. Dev.*, **65**, pp. 45-50 (2018).
- ¹¹W. Liu, B. Romanczyk, M. Guidry, N. Hatui, C. Wurm, W. Li, P. Shrestha, X. Zheng, S. Keller, U.K. Mishra *IEEE Microw. Wireless Compon. Lett.*, 1–1 (2021 6)
- ¹²M. Noshin, R. Soman and S. Chowdhury, *IEEE Electron Device Letters*, vol. **44**, no. 7, pp. 1072-1075, July (2023).
- ¹³M. Noshin, X. Wen, R. Soman, X. Xu, S. Chowdhury, *Appl. Phys. Lett.*, **123**, 6210 (2023).
- ¹⁴Z. Zhang, J. Singhal, S. Agrawal, E. Kim, V. Protasenko, M. Toita, H. G. Xing, D. Jena, *Appl. Phys. Lett.* **122**, 212106 (2023).
- ¹⁵Z. Zhang, J. Encomendero, E. Kim, J. Singhal, Y. Cho, K. Nomoto, M. Toita, H. G. Xing, and D. Jena, *Appl. Phys. Lett.* **121**, 082107 (2022).
- ¹⁶S. Keller, C. Suh, N. Fichtenbaum, M. Furukawa, R. Chu, Z. Chen, K. Vijayraghavan, S. Rajan, S. DenBaars, J. Speck et al., *J. Appl. Phys.* **104**, 093510 (2008).
- ¹⁷U. Singiseti, M. H. Wong, and U. K. Mishra, *Appl. Phys. Lett.* **101**, 012101 (2012).
- ¹⁸S. Diez, S. Mohanty, C. Kurdak and E. Ahmadi, *Appl. Phys. Lett.* **117**, 042102 (2020)
- ¹⁹B.S Eller, J. Yang, R.J Nemanich, *Journal of ELECTRONIC MATERIALS*, Vol. **43**, No. 12, (2014).
- ²⁰K.-S. Im et al., *IEEE Electron Device Letters*, vol. **31**, no. 3, pp. 192-194 (2010).
- ²¹U. Mishra, S. Likun, T. Kazior, Y.-F. Wu, GaN-based RF power devices and amplifiers. *Proc. IEEE* **96**, 287–305 (2008).
- ²²M. Matys; B. Adamowicz; A. Domanowska; A. Michalewicz; R. Stoklas; M. Akazawa; Z. Yatabe; T. Hashizume, *J. Appl. Phys.* **120**, 225305 (2016).
- ²³M. Matys, R. Stoklas, M. Blaho, B. Adamowicz, *Appl. Phys. Lett.* **110**, 243505 (2017).
- ²⁴J. A. Schuller, E. S. Barnard, W. S. Cai, Y. C. Jun, J. S. White, and M. L. Brongersma, *Nat. Mater.* **9**, 193 (2010).
- ²⁵M. L. Brongersma and V. Shalaev, *Science* **328**, 440 (2010).
- ²⁶J. Son, S. Rajan, S. Stemmer, and S. J. Allen, *J. Appl. Phys.* **110**, 084503 (2011).
- ²⁷M. Boucherit, O. Shoron, C. A. Jackson, T. A. Cain, M. L. C. Buffon, C. Polchinski, S. Stemmer, and S. Rajan, *Appl. Phys. Lett.* **104**, 182904 (2014).
- ²⁸K. Ahi, *Opt. Eng.*, vol. **56**, no. 9, Sep. (2017).
- ²⁹H. Spisser, A.-S. Grimault-Jacquin, N. Zerounian, A. Aassime, L. Cao, F. Boone, H. Maher, Y. Cordier, and F. Aniel, *J. Infrared Millim. Terahertz Waves* **37**, 243 (2015).
- ³⁰M. Bauer et al., *IEEE Trans. Terahertz Sci. Technol.*, vol. 9, no. 4, pp. 430-444, Jul. (2019).
- ³¹S. Boppel et al., *IEEE Trans. Terahertz Sci. Technol.*, vol. 6, no. 2, pp. 348-350, Mar. (2016).
- ³²Dyakonova, N.; Faltermeier, P.; But, D.B.; Coquillat, D.; Ganichev, S.D.; Knap, W.; Szkudlarek, K.; Cywinski, G., *J. Appl. Phys.* (2016), **120**, 164507.
- ³³Cibiraitė, D.; Bauer, M.; Ramer, A.; Chevtchenko, S.; Lisauskas, A.; Matukas, J.; Krozer, V.; Heinrich, W.; Roskos, H.G. Enhanced performance of AlGaIn/GaN HEMT-Based THz detectors at room temperature and at low temperature. In *Proceedings of the 42nd International Conference on Infrared, Millimeter, and Terahertz Waves (IRMMW-THz)*, Cancun, Mexico, 27 August–1 September 2017; pp. 1–2.
- ³⁴Shur, M.: AlGaIn/GaN plasmonic terahertz electronic devices. *J. Phys. Conf. Ser.* **486**, 012025 (2014).